



Rational design to manganese and oxygen co-doped polymeric carbon nitride for efficient nonradical activation of peroxymonosulfate and the mechanism insight

Chao He^a, Wu Xia^a, Chengyun Zhou^{a,*}, Danlian Huang^a, Chen Zhang^a, Biao Song^a, Yang Yang^a, Jun Li^b, Xing Xu^c, Yanan Shang^c, Li Du^a

^a College of Environmental Science and Engineering, Hunan University and Key Laboratory of Environmental Biology and Pollution Control (Hunan University), Ministry of Education, Changsha 410082, PR China

^b State Key Laboratory of Hydraulics and Mountain River Engineering, College of Water Resource & Hydropower, Sichuan University, Chengdu 610065, PR China

^c Shandong Key Laboratory of Water Pollution Control and Resource Reuse, School of Environmental Science and Engineering, Shandong University, Jinan 250100, PR China

ARTICLE INFO

Keywords:

Polymeric carbon nitride
Mn and O doped
Peroxymonosulfate
Enrofloxacin
Water treatment

ABSTRACT

Polymeric carbon nitride (PCN) based materials have emerged as promising catalysts to activate peroxymonosulfate (PMS) for organic pollutant removal. In this work, the Mn and O co-doped polymeric carbon nitride (Mn/O-PCN) was synthesized via simple calcination and activated PMS for enrofloxacin (ENR) removal. The obtained Mn/O-PCN + PMS system exhibited excellent reactivity for ENR degradation. The Mn and O dopants could modulate the electronic structure of PCN. ENR can be oxidized by electrons transferring and ¹O₂ on the surface of Mn/O-PCN + PMS complex via a non-radical way. A positive correlation was observed between ENR oxidation rates and the Mn content. Effects of pH, PMS concentration, and different ions on the degradation of ENR have also been studied. Cycling experiments showed that Mn/O-PCN materials have good reusability. Our study reported an effective PMS activator for organic pollutants removal and revealed the mechanism of active sites in modified PCN during non-radical PMS activation.

1. Introduction

Water pollution caused by refractory organic contaminants poses a potential threat to the ecological environment and humanity [1,2]. Enrofloxacin (ENR), a representative of fluoroquinolone antibiotics, has been extensively used in human and animal drugs in the past decades [3]. The majority of ENR and their metabolites entering the water environment due to the metabolic deficiency in human and animals. The residue ENR can potentially threaten the aquatic ecosystem and human health. Scientists have carried out researches on studying the remediation of refractory organic pollutants in water, such as microbial remediation, adsorption, photocatalytic oxidation and advanced oxidation processes (AOPs) [4–6]. Photocatalytic oxidation has mild reaction conditions and strong oxidation capacity, but its degradation performance is affected by the light transmittance of wastewater [7]. AOPs are one of the most attractive technologies for the degradation and detoxification of emerging water pollutants, which will generate the strong

reactive oxygen species and mineralize organic pollutants [8–10]. The current researches on typical oxidants are mainly H₂O₂, O₃, peroxymonosulfate (PMS) and peroxydisulfates (PDS). Compared with H₂O₂ or O₃, PMS and PDS have the advantages of low cost, high reactivity, and good stability properties [11].

The reaction rate of PDS and PMS are low when they directly react with the organic contaminants. Thus, activation is necessary for PDS and PMS when treating the organic contaminants. PMS or PDS can be activated by ultrasonic, heat, ultraviolet irradiation, and heterogeneous catalysts [12,13]. The activation of PMS by heterogeneous catalysts has attracted wide attention in solving environmental problems, especially in repairing organic pollution of soil and water [14,15]. Among these catalysts, manganese oxides (MnO_x) are recognized as a promising alternative due to their low toxicity and wide distribution of raw materials. Saputra et al. reported excellent catalytic performance of MnO₂ in the PMS activation for phenol removal [16]. Zhao et al. demonstrated that the Mn₃O₄-MnO₂/PMS system displayed strong catalytic

* Corresponding author.

E-mail address: zhouchengyun@hnu.edu.cn (C. Zhou).

<https://doi.org/10.1016/j.cej.2021.132751>

Received 3 August 2021; Received in revised form 23 September 2021; Accepted 28 September 2021

Available online 3 October 2021

1385-8947/© 2021 Elsevier B.V. All rights reserved.

performance to degrade ciprofloxacin [17]. However, the metal oxide has the poor chemical and thermal stabilities with the risk of metal ions leaching, which restricts their widespread applications [18,19]. In order to improve the stability of metal oxides, metal ion coordination complexes with N-based ligands is a feasible strategy [20].

In recent years, carbonaceous nanomaterials (such as graphene, carbon nanotubes, etc.) have been used as a new kind of nonmetallic materials for PMS activation and degradation of organic pollutants [21,22]. Polymeric carbon nitrides (PCN) as a conjugated polymer, which has a stable structure with rich nitrogen atoms, chemical stability, and cost-effective characters [23,24]. PCN were reported to activate PMS via a non-radical way, but the activity was restricted by the low electron transport ability [25]. Oxygen doping was proven to regulate the electronic structure of PCN and enhanced catalytic activity in PMS activation for the degradation of organic pollutants [26]. However, the catalytic efficiency of O-PCN was still limited due to the low oxidative potential. The N-rich environment of PCN can provide sufficient N atoms to coordinate with various metals (such as Fe, Co, Mn and Cu), which significantly improves the catalytic activity [27,28]. Due to the excellent redox performance of the central metal atom, PMS can be activated through a unique non-free radical pathway [29,30]. For example, Chen and coworkers reported that Fe and O co-doped PCN could activate PMS via a non-radical way for degradation of bisphenol A (BPA) [31]. With this mind, it can be expected that Mn and O co-doped PCN could have good catalytic activity and stability for activating PMS. However, in the process of activating PMS, the redox cycle mechanism of Mn(IV)/Mn(III)/Mn(II) is more complicated than Fe(III)/Fe(II), Cu(II)/Cu(I), etc. Therefore, the underlying mechanism of Mn coordination complexes with N-based ligands in PMS system also needs to elucidate.

In this study, urea was used as raw material, and different amounts of oxalic acid and manganese chloride were added in the calcination process to achieve structure control, and a series of manganese and oxygen co-doped polymeric carbon nitride (Mn/O-PCN) catalysts were prepared. The enrofloxacin (ENR) was selected as the target organic pollutants. In view of the current situation of antibiotic micro pollution in the water, the adsorption and degradation performance of Mn/O-PCN + PMS system for ENR removal were investigated. Influential factors properties of Mn/O-PCN for ENR removal have been evaluated. The types and contributions of reactive oxygen species and nonradicals produced in the system were studied. The possible catalytic active sites and catalytic mechanism of Mn/O-PCN were analyzed. In addition, the degradation path of ENR were further studied. In addition, the effect of different solution chemistry (pH, anions and cationic) on the activity of these reaction system has been discussed.

2. Experimental section

2.1. Synthesis of Mn/O-PCN

Urea, manganese chloride tetrahydrate ($\text{MnCl}_2 \cdot 4\text{H}_2\text{O}$), oxalic acid, Oxone (PMS, $2\text{KHSO}_5 \cdot \text{KHSO}_4 \cdot \text{K}_2\text{SO}_4$), $\text{K}_2\text{S}_2\text{O}_8$ (PDS), H_2O_2 solution (30%), furfuryl alcohol (FFA), and methanol (MeOH) were purchased from Sinopharm Chemical Reagent Co., Ltd, China. All chemicals were analytical grade and used without additional purification. Deionized water with a resistivity higher than $18.2 \text{ M}\Omega/\text{cm}$ was used in these experiments.

Manganese and oxygen co-doped polymeric carbon nitride (Mn/O-PCN) catalysts were synthesized according to a modified method [28]. 20 g of urea, 8 g of oxalic acid, and a certain amount (i.e., 0.1, 0.2, or 0.4 g) of $\text{MnCl}_2 \cdot 4\text{H}_2\text{O}$ were first mixed by ball milling. The obtained mixture was then placed in a crucible with a lid and the crucible was covered with a 3-layer aluminum foil [31]. The mixture was heated to 550°C at $2.3^\circ\text{C min}^{-1}$ and kept for 4 h under air condition. The products were washed with water and ethanol for three times. Different dosage of $\text{MnCl}_2 \cdot 4\text{H}_2\text{O}$ (i.e., 0.1, 0.2, or 0.4 g) was added to form the products and denoted as Mn/O-PCN-0.1, Mn/O-PCN-0.2 and Mn/O-PCN-0.4,

respectively. For comparison, PCN, O-PCN, and Mn-PCN were prepared by the same procedures without adding oxalic acid/ $\text{MnCl}_2 \cdot 4\text{H}_2\text{O}$, $\text{MnCl}_2 \cdot 4\text{H}_2\text{O}$, and oxalic acid, respectively.

2.2. Characterizations

X-ray diffraction (XRD, Bruker D8 Advance X-ray diffractometer) was used to examine the crystallography of PCN and modified samples. The morphology of Mn/O-PCN was tested by scanning electronic microscopy (SEM, QUANTA Q400, FEI) and transmission electron microscopy (TEM, G2F20, FEI). The chemical states of Mn/O-PCN were carried out on an X-ray photoelectron spectroscopy (XPS, ESCALAB 250 spectrometer, Thermo). The signal of free radicals were obtained by electron-paramagnetic resonance (EPR, JES-FA 200, JEOL) spectrometer with the spin reagent 2,2,6,6-Tetramethyl-4-piperidone (TEMP).

2.3. Evaluation of the catalytic performance

Enrofloxacin (ENR) degradation tests were carried out in a 100 mL flask under magnetic stirring. In a typical experiment, 15 mg of catalyst was added into the 50 mL of ENR solution (10 mg L^{-1}). Most of the reactions were conducted at initial pH 7.3. No buffer was applied for this pH. Then the mixture was stirred for 30 min to reach the adsorption-desorption equilibrium. The oxidation reaction experiments were then initiated by adding 0.2 mL of PMS stock solution (0.5 M) at the desired pH and stirred. At predetermined time intervals, the samples (about 1 mL) were withdrawn, filtered through a $0.22 \mu\text{m}$ polyethersulfone (PES) filter, and 0.02 mL of $\text{Na}_2\text{S}_2\text{O}_3$ (0.1 M) was injected to quench the reaction. The effects of coexisting anions on ENR removal were investigated in the presence of single anions and cationic. For the recycle runs of ENR degradation, the used catalyst was collected by centrifugation, washed ultrapure water and ethanol and dried overnight. Due to the small particle sizes, certain catalyst loss was unavoidable during the washing and drying processes. The concentration of ENR was analyzed using a high-performance liquid chromatography (HPLC, Agilent 1260) with a C18 column. The mobile phase consisted 40% methanol and 60% water (containing 0.1% formic acid) and the flow rate was 1.0 mL min^{-1} . The detection wavelength was 278 nm. The degradation products of ENR were examined by the liquid chromatography mass spectrometry (LC-MS, Agilent). The detailed method was originated from the literature [32,33].

2.4. Electrochemical measurements

All electrochemical measurements were conducted on an electrochemical workstation (CHI 760E, China) with a three-electrode system [34]. The three-electrode system was consist of working electrode (catalysts deposited on glassy carbon electrode), counter electrode (Pt plate), and the reference electrode (Ag/AgCl). The working electrode was prepared as follows: the catalyst (about 2 mg) was suspended in a mixture solution containing 0.1 mL of 5 % Nafion and 0.9 mL ethanol solution. Then the mixture was sonicated about 30 min and dropped 20 μL of mixture onto the GCE electrode. The working electrode was then dried at ambient temperature. Electrochemical impedance spectroscopy (EIS) was performed at the open potential in 0.2 M Na_2SO_4 solution with the frequency ranging from 10^{-1} to 10^5 Hz. The potential of PCN-PMS complexes was measured via chronopotentiometry analysis.

3. Results and discussion

3.1. Characterization of Mn/O-PCN

As illustrated in Fig. 1a, the XRD patterns of PCN shows the typical $\text{g-C}_3\text{N}_4$ peaks, including two representative peaks at 12.7° and 27.4° corresponded to the (100) in-plane periodic repeat structural and the conjugated aromatic systems in (002) graphitic planes, respectively.

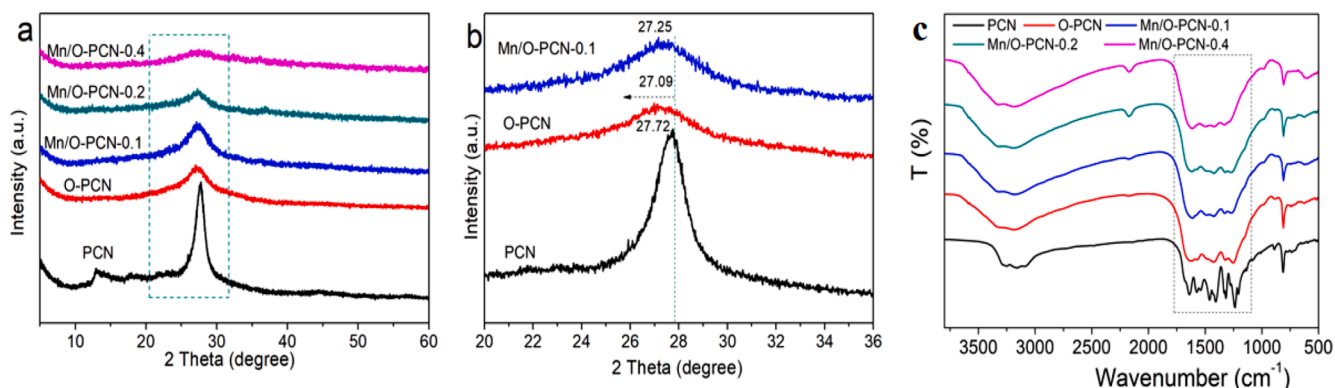


Fig. 1. (a) Powder XRD patterns of as-prepared samples, (b) magnification of the corresponding (002) peak, (c) FTIR pattern of as-prepared samples.

After doping with OA, the peaks of O-PCN were broadened due to the incorporation of oxygen. With the increasing amount of MnCl_2 in PCN, the peak intensity of (100) and (002) was decreased due to the modification of MnCl_2 . Fig. 1b showed a partial enlarged picture of Fig. 1a. The (002) peak of modified PCN had some deviation, which indicated that nitrogen atoms in different chemical environment of PCN may change. In addition, no new typical peaks related to manganese oxides, manganese chlorides and manganese carbides were found, indicating that Mn may present Mn-N coordination in the PCN. The FTIR spectra of the prepared PCN, O-PCN, and Mn/O-PCN-x materials were illustrated

in Fig. 1c. For PCN, the peaks from 1200 to 1600 cm^{-1} were corresponded to the stretching of heterocycles and the peaks at 804 cm^{-1} was attributed to the heptazine core [35]. Compared with PCN, the peaks at 804 cm^{-1} of O-PCN and Mn/O-PCN-x materials showed a weakened intensity due to the oxygen doping.

The morphology of PCN and Mn/O-PCN-0.2 was studied by SEM and TEM. As shown in Fig. 2a and b, the SEM image of PCN and Mn/O-PCN-0.2 presents a layered and platelet-like structure. The EDS element mapping results showed that the elements of C, N, O and Mn were evenly distributed in Mn/O-PCN-0.2, which confirmed that the Mn and O were

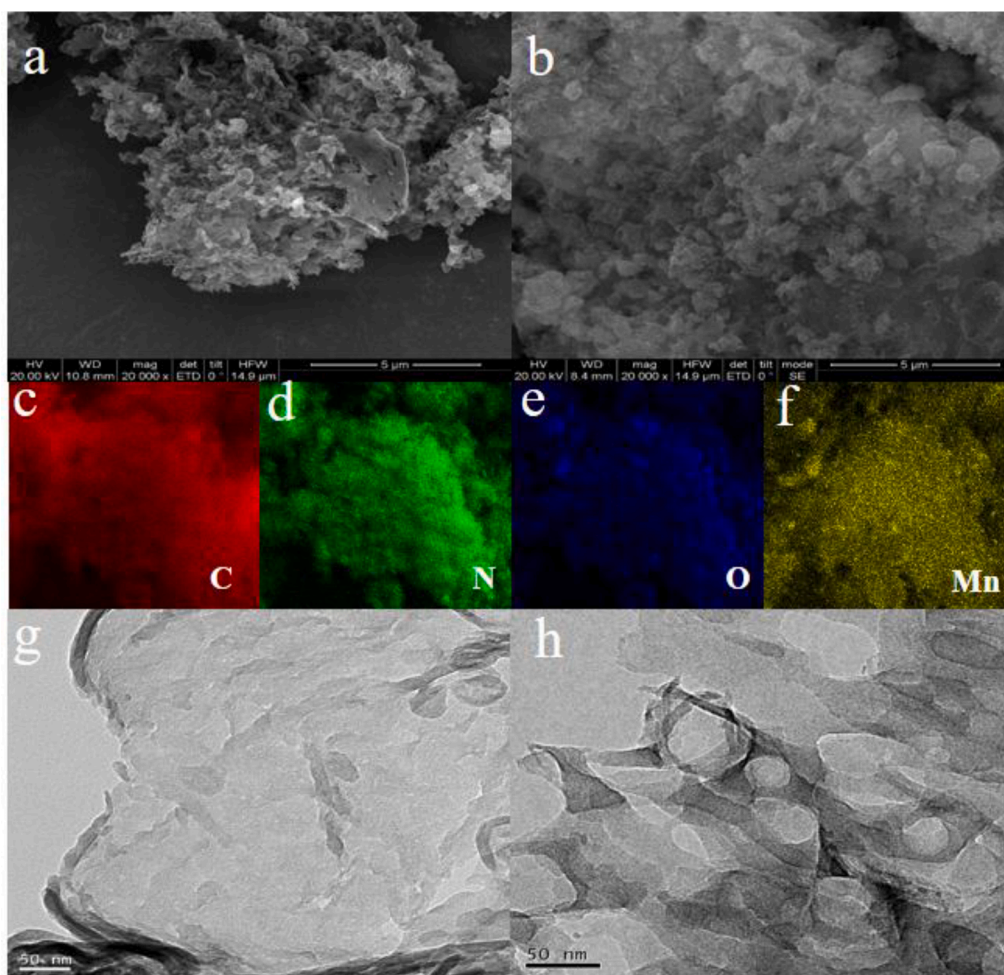


Fig. 2. SEM images of (a) PCN and (b) Mn/O-PCN; SEM-EDS mapping images of the Mn/O-PCN (c) C, (d) N, (e) O and (f) Mn and TEM images of (g) PCN and (h) O-PCN.

successfully doped into the PCN (Fig. 2c–f). The actual amount of Mn in Mn/O-PCN-0.1, Mn/O-PCN-0.2, Mn/O-PCN-0.4 was 1.21%, 2.52% and 4.93% by ICP-MS, respectively. The TEM image of PCN also showed a typical layer structure, while the Mn/O-PCN-0.2 remained the nano-sheets with some irregular holes (Fig. 2g–h). Fig. S1 shows the TEM-EDS analysis further confirming the presence of C, N and Mn on the surface of Mn/O-PCN-0.2. As illustrated in Fig. S2, the N₂-adsorption curve of PCN samples could be fitted H3 hysteresis. The H3 hysteresis suggested the presence of plate-like particles, which was consistent with SEM image. The surface area of O-PCN was higher than PCN, which was due to the existence of mesoporous in O-PCN. However, the surface area of Mn/O-PCN-0.2 was decreased to 52.83 m²/g, which was lower than that of PCN (68.76 m²/g) (Table 1). This was probably due to the doped of Mn restricted the polymerization of urea [30]. The average pore diameter of Mn/O-PCN-0.2 was 1.19 nm, which indicated the pore mainly consisted of mesoporous.

The chemical composition of the Mn/O-PCN-0.2 was determined via XPS spectra. The presence of C, N, O and Mn on the surface of Mn/O-PCN-0.2 was observed from XPS survey scan (Fig. S3). As shown in Fig. 3a, the high-resolution Mn 2p of Mn/O-PCN-0.2 was observed the 2p_{3/2}–2p_{1/2} doublet at 641.7 and 653.8 eV [36,37]. In the Mn 2p_{3/2} spectrum, the peaks around 641.2, 642.4 and 643.4 eV were assigned to Mn (III), Mn (IV) and Mn (II), respectively [17]. In Fig. 3b, the N1s spectra can displays three respectively correspond to pyridinic N (398.5 eV), pyrrolic N (399.2 eV) and graphitic N (400.4 eV). As shown in Fig. 3c, the C1s spectra displayed four peaks corresponding to sp²-hybridized carbon bonds N=C–N (284.8 eV), C–O bonds (285.3 eV), adventitious C=O/O–C–O bond (287.1 eV), and N=C–O (288.1 eV), respectively [28]. In the O 1s spectra, the peak at 531.3 eV corresponding to surface adsorbed water, while the other two novel peaks corresponding to physically adsorbed oxygen (529.9 eV) and the introduced C–OH group (531.9 eV) (Fig. 3d) [38]. Compared with PCN, the ratio of N/C for Mn/O-PCN-0.2 decreased from 1.09 to 0.86, while the proportion of O for Mn/O-PCN-0.2 obviously increased from 3.57% to 8.77% (Table S1). The above results indicated that part of nitrogen atoms in Mn/O-PCN-0.2 was substituted by oxygen atoms.

3.2. Mn/O-PCN-x catalytic performances for PMS activation to removal ENR

ENR was hardly oxidized by PMS without catalyst. Fig. S4 showed the adsorption efficiency of ENR by different catalysts. The results showed that the adsorption efficiency of different catalysts for ENR are similar. After adsorption, the concentration of ENR in each flask was about 7.8–8.1 mg/L. The removal efficiency of ENR by pure PCN and PMS was about 22% in 45 min. However, in the presence of O-PCN and PMS, the removal efficiency of ENR was increased to 42% (45 min) (Fig. 4a). The Mn/O-PCN catalyst exhibited excellent catalytic activity to activate PMS for ENR removal and the removal efficiency of this system was reached above 99% in just 20 min. The ENR degradation performances fitted well with the pseudo-first-order kinetic model. The kinetic value of Mn/O-PCN-0.2 was 0.144 min⁻¹, followed by O-PCN (0.066 min⁻¹), Mn-PCN (0.012 min⁻¹), and PCN (0.007 min⁻¹) (Fig. S5a). The results illustrated that the Mn/O-PCN has excellent catalytic activity toward PMS activation. As shown in Fig. 4b, the effects of MnCl₂ amount on ENR degradation were also examined. As the initial

MnCl₂ loading was increased from 0.1 to 0.2 g, the ENR degradation efficiency obviously increased from 58% to 75% in 10 min. However, when the content of MnCl₂ increased to 0.4 g, the degradation efficiency of ENR was not obviously increased. The reaction rate of Mn/O-PCN-0.1, Mn/O-PCN-0.2, and Mn/O-PCN-0.4 for ENR removal within 30 min was 0.095 min⁻¹, 0.144 min⁻¹, and 0.152 min⁻¹, respectively (Fig. S5b). It can be seen that the catalytic activity of Mn/O-PCN was not linearly related to the doping amount of MnCl₂.

Furthermore, the effect of PMS concentration and dosage of catalyst on the catalytic activity of Mn/O-PCN were also studied. In Fig. 4c, the Mn/O-PCN exhibited 10% of adsorption capacity toward ENR with the absence of PMS, indicating the activation of PMS is necessary. As the PMS dose increases from 1 mM to 3 mM, the degradation rate of ENR rises, which indicates that the removal rate depends on the PMS dose within the limits of 1–3 mM. However, the degradation rate after excessive PMS (5 mM) added. The results indicated that increasing the concentration of PMS in a certain range can produce more active free radicals to react with ENR, and further improve the reaction rate of ENR [39]. When the concentration of PMS is too high, the redundant PMS would react with oxidizing radicals, thus affecting the degradation activity of ENR [40]. The ENR degradation with different catalyst dosages was presented in Fig. 4d. The removal rate of ENR increased from 35% to 90% obviously within 10 min as the Mn/O-PCN dosage increased from 0.1 to 0.3 g L⁻¹. In addition, the effect of ENR concentration on Mn/O-PCN reaction system was also studied (Fig. S6). The ENR (5.0–15 mg/L) could be completely removed within 30 min and even 20 mg/L ENR could be achieve 90% after 45 min reaction. These above results suggest that the suitable MnCl₂ loading, PMS dosage, and catalyst dosage was beneficial to PMS utilization. In addition, the results also demonstrated that Mn/O-PCN has high catalytic activity to PMS for organic pollutant degradation.

The solution pH affects the functional groups of catalyst as well as radicals species. As shown in Fig. 5a, the ENR removal efficiency increased from pH 3.0 to 8.0, and then increased remarkably with pH further increase to 11 in the Mn/O-PCN/PMS system. The zeta potential and ENR species in different pH was listed in Fig. S7. The isoelectric point of Mn/O-PCN was 4.0 and the pKa of ENR was reported to be 6.16 and 8.23 [41]. The electrostatic repulsion between protonated ENR and the positively charged Mn/O-PCN may take place at pH < 4.0, and then inhibited the reaction. The enhanced removal efficiency of ENR at neutral or alkaline conditions was probably ascribed to that PMS was more conducive to being activated and SO₄^{•-} can be simultaneously converted into •OH under alkaline condition [42,43]. Inorganic ions may exist in the natural water environment, which may consume the radical species and further affect the removal efficiency of ENR [44]. The co-existing anions including Cl⁻, NO₃⁻, SO₄²⁻, CO₃²⁻ and PO₄³⁻ with 100 mM concentrations were added into the Mn/O-PCN-0.2/PMS system (Fig. 5b). The addition of Cl⁻ and CO₃²⁻ accelerated ENR degradation, which was due to the formation of hypochloric acid and the increased solution pH, respectively [45]. The NO₃⁻ and SO₄²⁻ present inhibited effects on the ENR degradation activity, which may due to the active radicals can be consumed and form the secondary radicals with lower oxidizing activity [46]. The presence of PO₄³⁻ inhibition on the ENR degradation, resulting in a decrease in the ENR removal from 100% to 40% at 100 mM of PO₄³⁻. The PO₄³⁻ may coordinate with the central metal ions to reduce the catalytic activity. In addition, heavy metal may adsorb in the catalyst surface and occupy the reactive sites in practical applications. However, the results indicated that the heavy metal (i.e. Cu²⁺) had a negligible effect on ENR degradation in the Mn/O-PCN/PMS system [47]. In addition, a series of HA (1 and 5 mg/L) was added to ENR solution to evaluate the effect of NOM on the degradation activity of catalysts (Fig. S8). The addition of HA showed a slight effect on ENR removal. When the concentration of HA was 1 mg/L, the ENR degradation efficiency was slightly affected. For higher concentration of HA, the HA could accelerated pollutant degradation, which may attributed to the quinone group of HA promote the activation of PMS to

Table 1
surface area and pore volume for PCN and LCN-x samples.

Samples	Surface area (m ² g ⁻¹)	Pore volume (cm ³ g ⁻¹)	Pore diameter (nm)
PCN	68.76	0.49	2.74
O-PCN	78.06	0.37	4.43
Mn/O-PCN-0.2	52.83	0.38	1.19

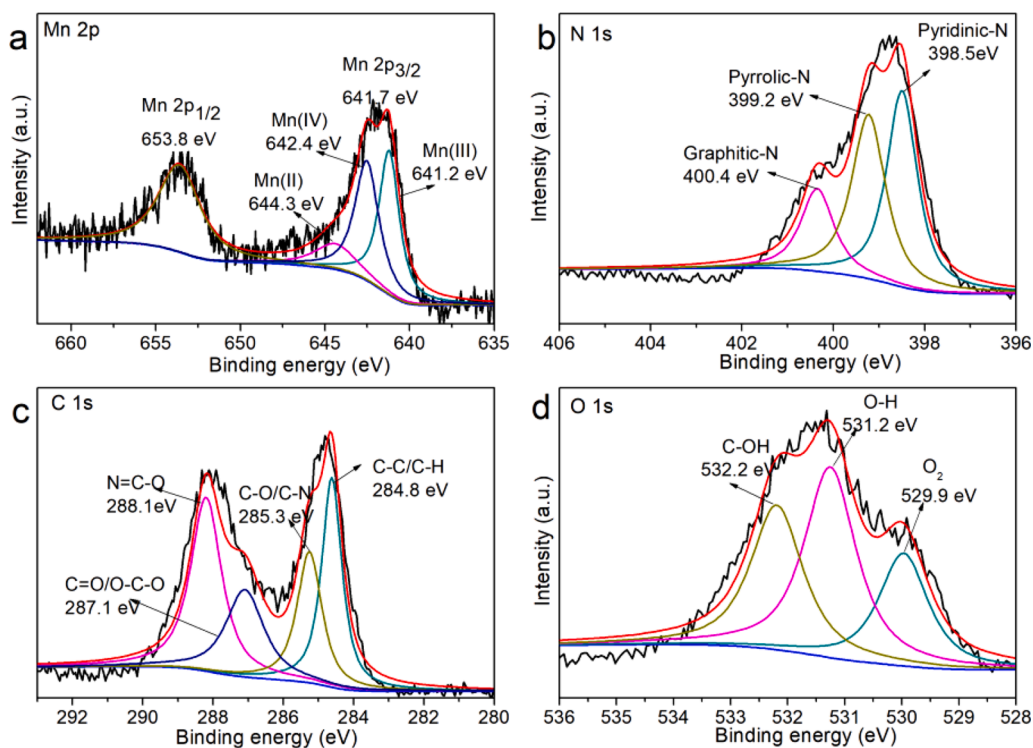


Fig. 3. XPS spectra of Mn/O-PCN-0.02, (a) Mn 2p, (b) N 1 s, (c) O 1 s and (d) C 1 s.

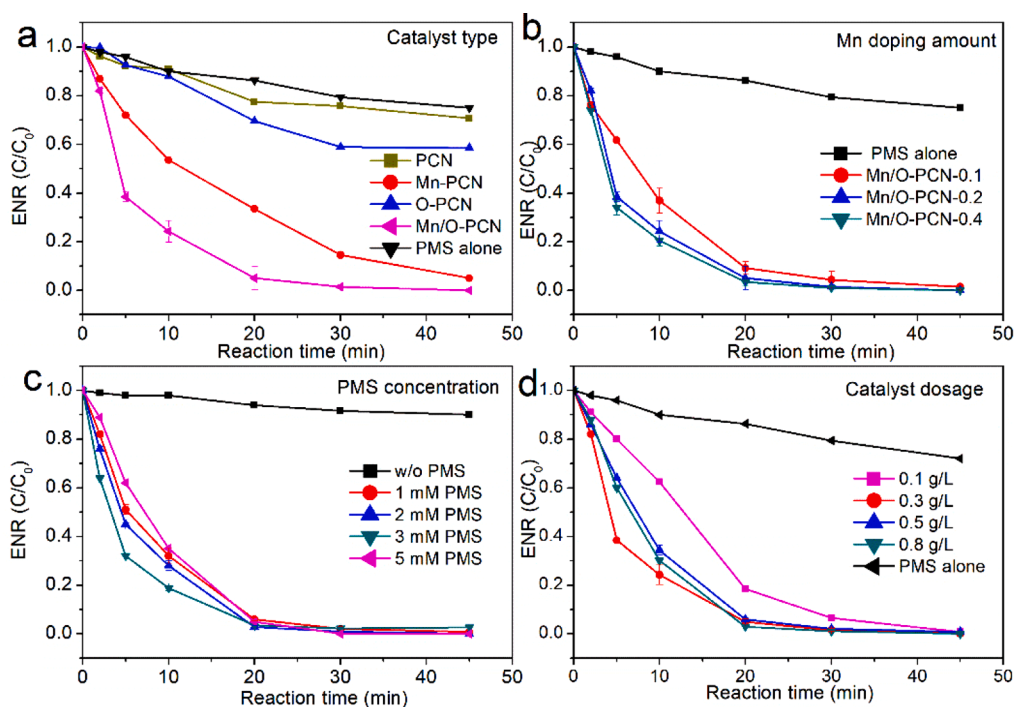


Fig. 4. (a) Degradation of ENR in PMS-based AOPs catalyzed by different PCN catalysts (reaction conditions: $[PMS]_0 = 1 \text{ mM}$, $C(ENR)_0 = 10 \text{ mg L}^{-1}$, $C(\text{catalyst}) = 0.3 \text{ g L}^{-1}$, $T = 25 \text{ }^\circ\text{C}$, initial $\text{pH} = 6.81$); effects of (b) MnCl_2 content, (c) PMS concentration, (d) catalyst dosage on the removal of ENR.

produce more active free radicals [48].

Different oxidants (PMS, PDS, and H_2O_2) on the catalytic activity of Mn/O-PCN-0.2 were also investigated. As shown in Fig. 5c, Mn/O-PCN-0.2 exhibits higher catalytic performance with PMS than with PDS activation. This results may be attributed to the difficulty in breaking O—O bonds in a symmetrical structure of PDS. In addition, Mn/O-PCN-

0.2 cannot activate H_2O_2 which is due to the stronger bond energy of O—O in H_2O_2 than PMS. The potential of Mn/O-PCN for pollutant degradation in practical applications was further measured in lake water and tap water. In tap water and lake water, the degradation efficiency of ENR can also reach nearly 100% within 45 min (Fig. 5d), which may due to the non-radical system can adapt to the interference by background

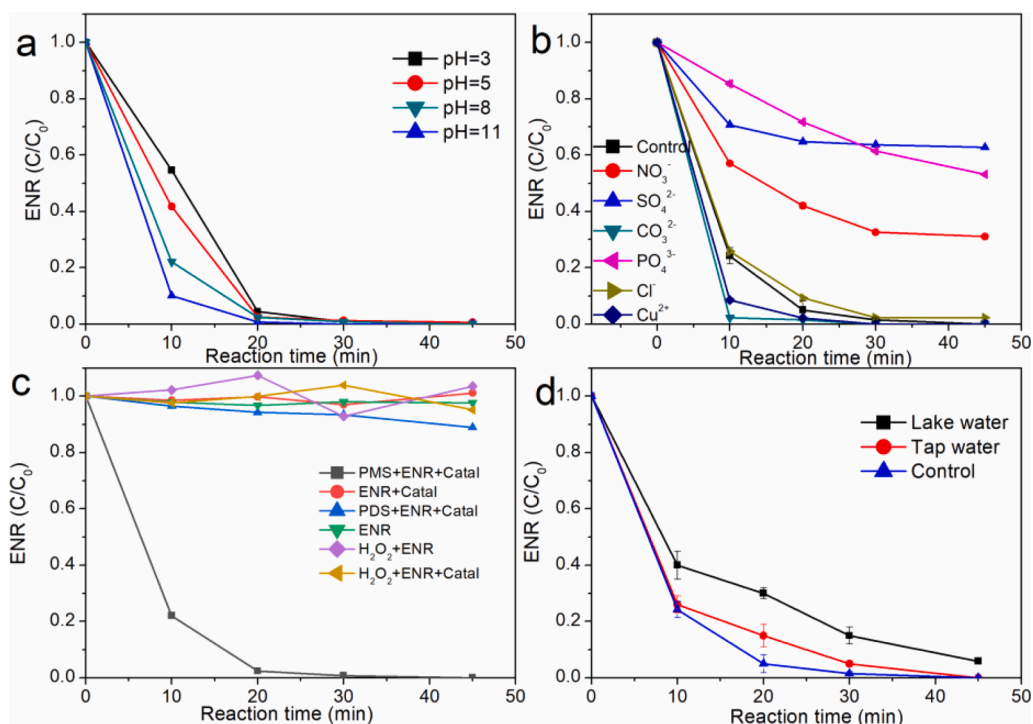


Fig. 5. (a) Effects of pH, (b) effects of the coexisting anions, (c) effects of different oxidant, (d) effects of water matrix on the ENR degradation efficiency of the Mn/O-PCN-0.02 + PMS system (reaction conditions: [PMS]₀ = 1 mM, C(ENR)₀ = 10 mg L⁻¹, C(catalyst) = 0.3 g L⁻¹, T = 25 °C).

inorganic and organic matter.

3.3. Degradation mechanism

Generally, radicals (e.g., SO₄^{•-} and •OH) are considered as the main reactive species in PMS activation processes. Besides radicals, non-

radicals way (e.g., electron transfer or ¹O₂ generation) has also been reported [49]. To clarify the major reactive species in Mn/O-PCN + PMS system, trapping experiments were carried out. Tert-butanol (TBA), methanol, and ethanol were carried out to confirm the presence of •OH and SO₄^{•-}. As shown in Fig. 6a, when methanol was added into the Mn/O-PCN/PMS system, the degradation activity of ENR showed a little

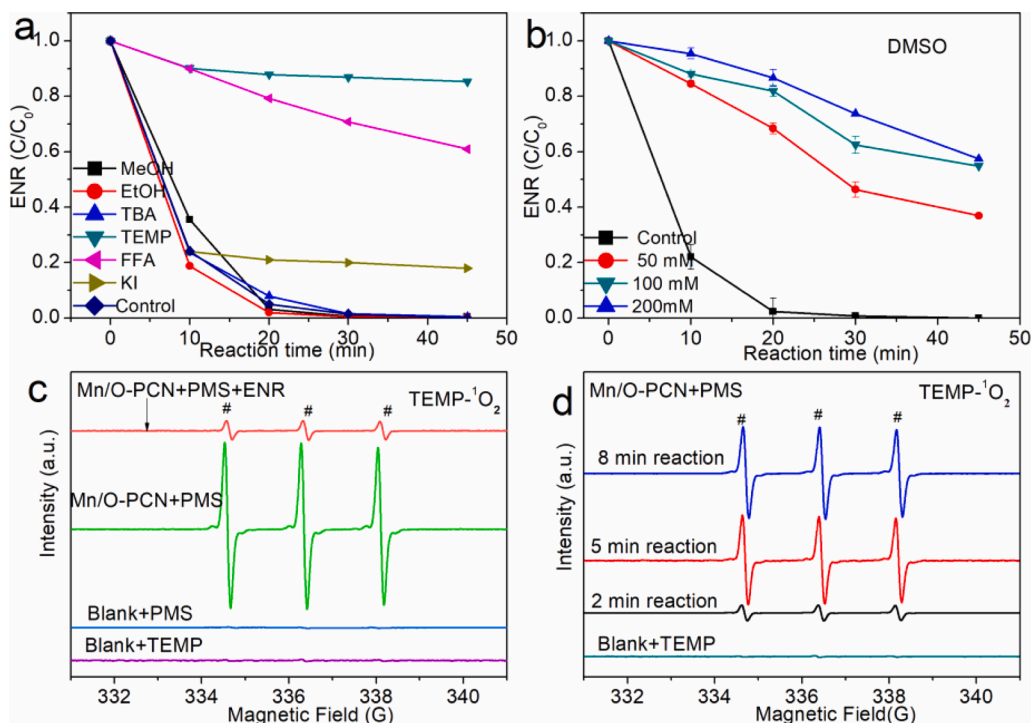


Fig. 6. (a) Quenching experiments on ENR degradation in the Mn/O-PCN-0.02 + PMS system, (b) Effect of DMSO on ENR degradation in the Mn/O-PCN-0.02 + PMS system, (c) TEMP-¹O₂ spectra in different conditions, (d) ESR spectra of Mn/O-PCN-0.02 + PMS system in different reaction time (reaction conditions: [PMS]₀ = 1 mM, C(ENR)₀ = 10 mg L⁻¹, C(catalyst) = 0.3 g L⁻¹, T = 25 °C, initial pH = 6.81).

inhibition, which indicates that the $\bullet\text{OH}$ and $\text{SO}_4^{\bullet-}$ may not possess the main role in this system. The removal efficiency of ENR was still higher than 95% with the addition of TBA. The results suggested a non-radical pathway may exist in the Mn/O-PCN + PMS system [50]. However, the addition of FFA (200 mM) significantly suppressed ENR degradation, and the final removal efficiency was only 24.3% within 45 min [51]. It can be inferred that $^1\text{O}_2$ may act as the major reactive species in the Mn/O-PCN + PMS system. In addition, the presence of TEMP decreased the ENR removal efficiency from 99% to 15% within 45 min. These above results illustrated that PMS could be activated by Mn/O-PCN mainly based on $^1\text{O}_2$ generation instead of $\text{SO}_4^{\bullet-}$ and $\bullet\text{OH}$. Previous studies pointed that potassium iodide (KI) can act as a quencher for the surface bound reactive species. The addition of KI could partially inhibit the removal efficiency of ENR, which suggested that the ENR may react with $^1\text{O}_2$ via surface bound catalytic process [8].

Previous studies indicated that the central metal active sites (i.e. high valence Mn-oxo species) also play a key role in ENR removal processes. To confirm this possible way, dimethyl sulfoxide (DMSO) is often used as a probe reagent in the reaction system due to the DMSO can react with high valent metal oxides to form dimethyl sulfone (DMSO_2) [31]. With the addition of 50 mM DMSO, the degradation efficiency of ENR decreased obviously from 100% to nearly 60% (Fig. 6b). As the concentration of DMSO increase, the degradation efficiency of ENR was continuously inhibited. The above results suggested that $^1\text{O}_2$ and high-valent Mn species in the Mn/O-PCN/PMS system may play a vital role in the ENR degradation.

To further confirm the phenomenon observed in the trapping experiment, the TEMP as a spin trap with ESR test for capturing $^1\text{O}_2$ was then carried out. As shown in Fig. 6c, a weak intensity of three-line spectrum was found in the TEMP-water solution and TEMP-PMS solution. After the Mn/O-PCN was added, the typical strong three-line spectrum (hyperfine splitting of $\alpha_N = \alpha_N = \alpha_N = 16.9$ G) was observed. It seemed that the Mn/O-PCN + PMS system would generate the signal of TEMP- $^1\text{O}_2$. With the addition of ENR, the above signal in

Mn/O-PCN + PMS + ENR system was decreased, indicating that the $^1\text{O}_2$ was consumed by ENR [31]. Furthermore, the signal of TEMP- $^1\text{O}_2$ for Mn/O-PCN system in PMS activation was increased with the increase of reaction time (Fig. 6d).

Electron transfer was another non-radical oxidation way in some PMS activation reactions. Electrochemical impedance spectroscopy (EIS) of PCN and Mn/O-PCN were measured to explore the effect of Mn and O on the conductivity of catalyst. Previous studies indicated that the smaller arc radius on the EIS represents a more effective interfacial electron transfer of catalysts. As displayed in Fig. S9, the PCN showed a large diameter of arc radius, indicating high electron transfer resistance. While the plot of Mn/O-PCN-0.2 exhibited a small arc radius, which means excellent conductivity. Open-circuit potential of glassy carbon electrode (GCE) coated with Mn/O-PCN was also used to investigate the electron transfer among catalyst, PMS, and ENR (Fig. 7a). When PMS was injected in the electrolyte, the potential output suddenly increased due to the electron transfer from Mn/O-PCN to PMS [52]. The potential changed for Mn/O-PCN-0.1, Mn/O-PCN-0.2, Mn/O-PCN-0.4 was 0.145 V, 0.202 V, and 0.225 V, respectively. The PMS adsorption on Mn/O-PCN catalysts were presented in Fig. 7b. It seems that the Mn/O-PCN-0.4 has the highest adsorption capacity of ENR [25]. The correlation between PMS adsorption and the potential of Mn/O-PCN was significantly positive (Fig. 7c). The results illustrated that high content of Mn improve the interaction of Mn/O-PCN and PMS and produce more surface-bound complexes. In addition, the kinetic rate constants for ENR removal have a good relation with the potential of Mn/O-PCN (Fig. 7d). According to the results, the enhanced electron-transfer ability between PMS and Mn/O-PCN was benefit for the degradation of ENR [23,53].

To further explore the degradation mechanism of ENR, the intermediate products formed among this process were identified by using high performance liquid chromatography-mass spectrometer (HPLC-MS) in positive mode. The original spectrum of ENR and the degradation sample was shown in Fig. 8a. After degradation, the main peak of ENR disappeared and the new peaks were observed. The molecular weight of possible intermediates at different reaction time have been shown in

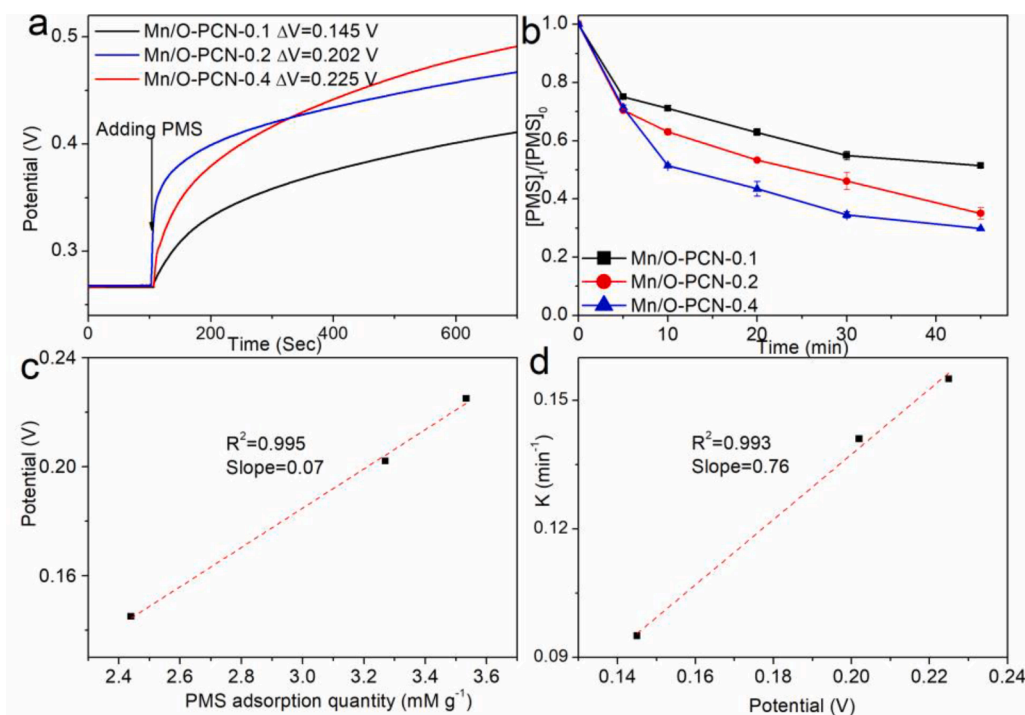


Fig. 7. (a) The changes of open-circuit potentials of Mn/O-PCN-x + PMS systems without ENR, (b) PMS adsorption on Mn/O-PCN-x catalysts, (c) correlation between the potential of surface complexes and PMS adsorption quantity, (d) correlation between k values and potential of surface complexes (reaction conditions: $[\text{PMS}]_0 = 1$ mM, $C(\text{ENR})_0 = 10$ mg L^{-1} , $C(\text{catalyst}) = 0.3$ g L^{-1} , $T = 25$ °C, initial pH = 6.81).

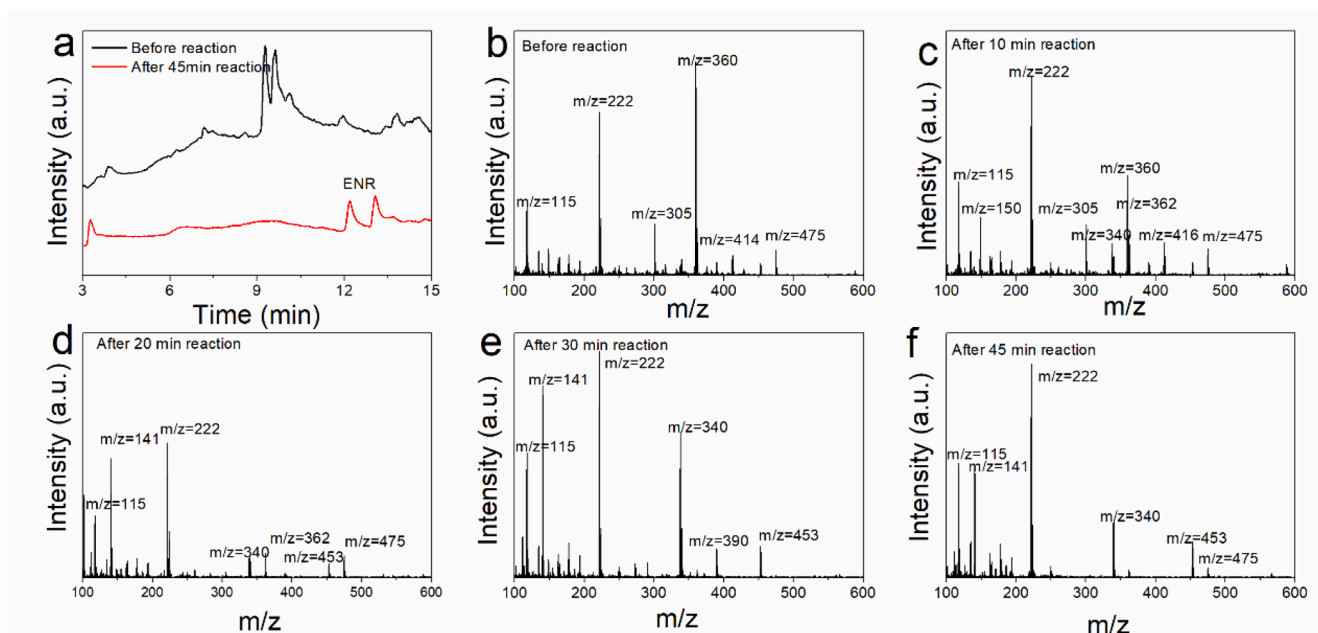


Fig. 8. (a) LC spectra of ENR before reaction and after reaction; Mass spectra of ENR in the Mn/O-PCN + PMS system under (b) 0 min, (c) 10 min, (d) 20 min, (e) 30 min, (f) 45 min reaction.

Fig. 8b–8f. As shown in Fig. 8b, the product ion at $m/z = 360$ was corresponding to ENR ($C_{19}H_{12}FN_3O_3$) before reaction. After 20 min reaction, the intensity peak of ENR was decreased, while the new peak at $m/z = 362, 340$ and 115 were observed (Fig. 8c and d). With the reaction time prolonging, these peaks located at $m/z = 340$ and 390 were first increased and then decreased (Fig. 8e and f), which indicated that the intermediates are being further decomposed.

Based on the previous studies and analysis, these product ions at $m/z = 362, 340, 390$ and 115 might identified as $C_{17}H_{16}FN_3O_5$, $C_{17}H_{16}N_3O_5$, $C_{19}H_{20}O_5FN_3$ / $C_{20}H_{27}O_5N_3$ and $C_5H_{12}NO_2$, respectively [54]. As shown in Fig. S10, the concentration of ENR ($m/z = 360$) decreased with the time increasing, indicating the ENR was degraded. The concentration of degradation products was increasing. Degradation pathway has been proposed based on the above results. In Fig. 9, the oxidative cleavage of piperazinyl and quinolone seems to occur simultaneously. The first

degradation pathway was similar to the previous reports. The P1 ($m/z = 390$) compound was obtained by the piperazine ring oxidation of ENR via 1O_2 . Further loss of one formaldehyde in the opened piperazine ring led to the formation of P2 ($m/z = 362$) compound. P3 ($m/z = 306$) compound was formed by the second formaldehyde elimination [55]. The second way includes de-fluorination and the cleavage of the quinolone moiety. P4 ($m/z = 340$) compound was probably generated due to the de-fluorination reaction. ENR undergo an OH substitution and oxidation step to open the quinolone moiety and formed P5 ($m/z = 390$) [56]. Finally, P5 was further oxidation to completely destroy the ENR structure and produced P6 ($m/z = 115$) and P7 ($m/z = 150$).

According to the above results, a possible mechanism was proposed in Fig. 10. Previous study indicated that the oxygen doping can modulate the electron distribution of PCN [57]. The oxygen dopants can increase the positive charge of nearby carbon atoms in Mn/O-PCN. The

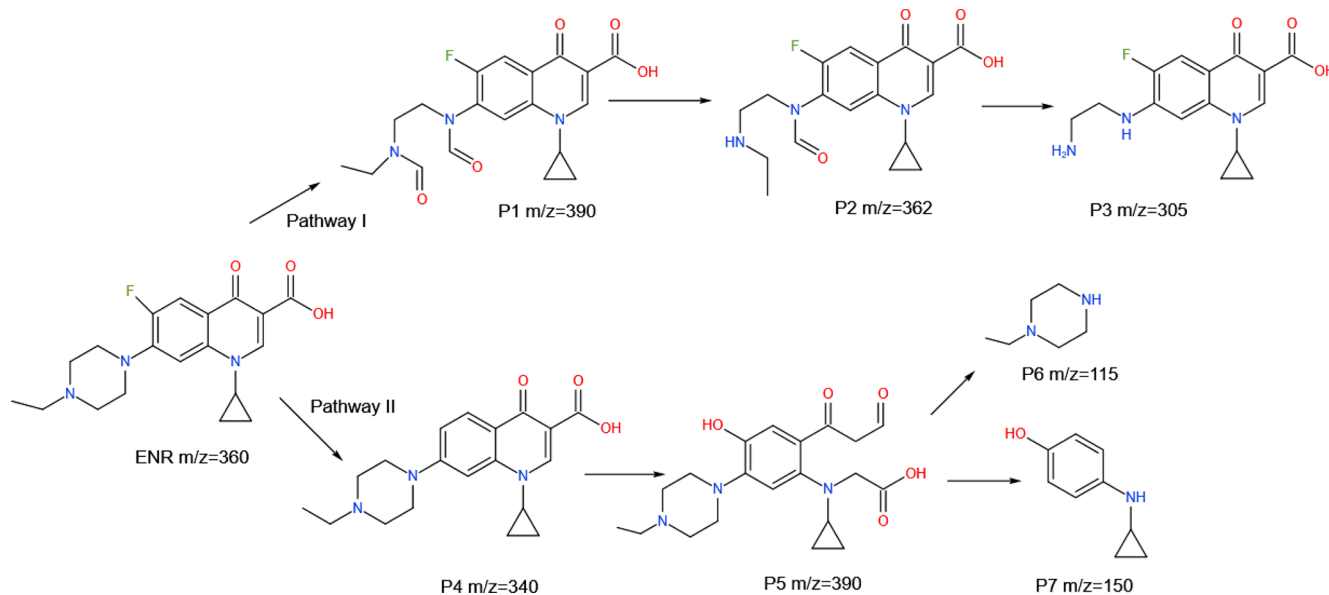


Fig. 9. Degradation pathways of ENR in the Mn/O-PCN + PMS system.

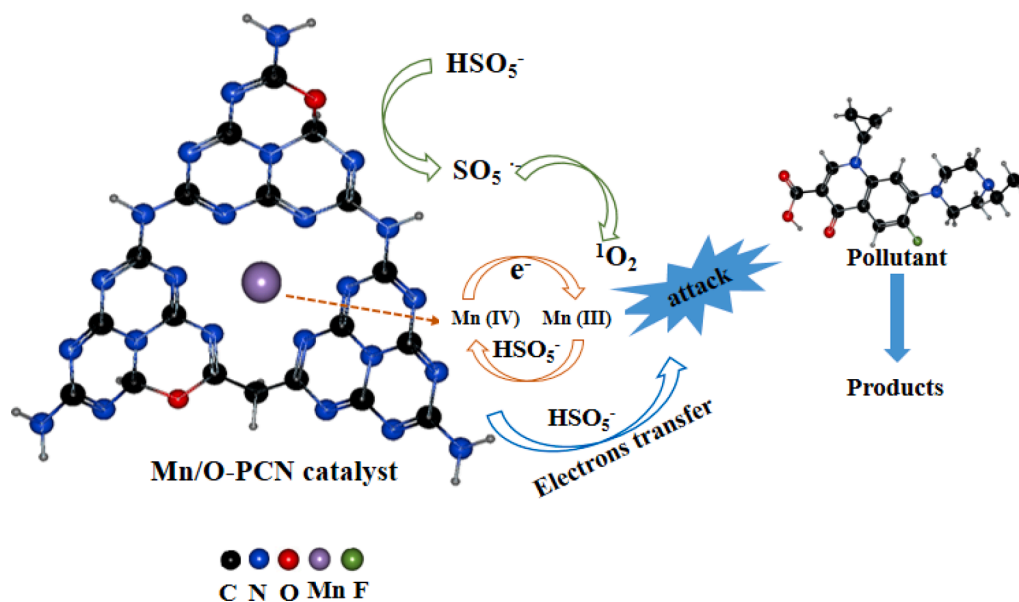


Fig. 10. Proposed mechanism behind PMS activation over the Mn/O-PCN toward organic pollutant oxidation.

surface electron could transfer from PMS (HSO_5^-) to the carbon atoms of PCN formed the $\text{SO}_5^{\bullet-}$, then the $\text{SO}_5^{\bullet-}$ would react with water to generate $^1\text{O}_2$ [26]. In addition, the O-PCN could act as an electron mediator, which could enhance the electron transfer between PMS and Mn (IV). In this case, Mn (IV) would be converted to Mn (III) via PMS activation. According to the simulation measurement, the longest diameter of ENR can reach 15 Å (1.5 nm) and the height can reach 8 Å (0.8 nm) (Fig. S11). The pore diameter of Mn/O-PCN-0.2 is 1.2 nm. Therefore, ENR molecules can enter the pore of the catalyst at a certain angle for catalytic reaction. Furthermore, PMS and ENR can be absorbed onto the Mn/O-PCN to form the Mn/O-PCN/PMS complex, and then the ENR can be oxidized by electrons transferring and $^1\text{O}_2$ to the above complex via a non-radical way [25].

3.4. Stability of Mn/O-PCN for the degradation of ENR

The stability of Mn/O-PCN was investigated by four cycling tests in pH 7.3. From Fig. S12, as high as 94% ENR removal was obtained after four cycles, suggesting the excellent stability of Mn/O-PCN catalyst. This change of degradation activity may be due to the intermediates occupying the reactive sites of catalyst. The concentration of dissolved Mn ions was also investigated. The concentration of dissolved Mn ions was 1.5 mg L^{-1} in the first round of reaction, which was only 6.0 wt% of total Mn content in the Mn/O-PCN-0.2. After four cycles, the concentration of dissolved Mn ions was hard to detect. According to the discharge standard for industrial pollutants in China (GB 8978–1996), the maximum manganese (Mn) concentration is 2 mg L^{-1} . Therefore, secondary pollution caused by material use can be ignored. The XRD, FT-IR, XPS and SEM image of fresh and used catalyst was measured (Fig. S13). The FT-IR, XRD spectra and SEM image of fresh and used Mn/O-PCN-0.2 showed no obvious changes, indicating that the structure and composition of Mn/O-PCN-0.2 were not destroyed after the reaction process, further indicating that the structure of the catalyst was stable. In addition, the change of chemical composition and structure were characterized by XPS analysis. In the Mn 2p XPS spectra, the binding energy of Mn (III) and Mn (IV) increased by 0.6 and 0.4 eV, respectively. In the N1s XPS spectra, the binding energy of pyridinic-N and graphitic-N decreased by 0.2 eV and the content of graphitic N increased from 19% to 24% (Fig. S14). The increase of binding energy indicates the nature of electron donor, while the decrease of binding energy indicates the electron acceptor property [28]. As a result, the nitrogen and Mn (IV)

could be as active sites for PMS activation. The variation in binding energy indicated the occurrence of electron transfer. These results demonstrated that the excellent stability of the Mn/O-PCN photocatalyst has been prepared and it could be applied in practical applications.

4. Conclusions

In this study, the Mn and O co-doped polymeric carbon nitride (Mn/O-PCN) material was prepared by high-temperature carbonization under air condition. The Mn doping provides more active sites, while oxygen doping can modulate the electronic property of PCN. The obtained Mn/O-PCN exhibit excellent activities and stabilities for catalytic oxidation of ENR with PMS as an oxidant. The Mn/O-PCN has good applicability in the wide pH range of 3–11, and the catalytic performance was further enhanced in the presence of Cl^- . The kinetic rate constants for ENR removal have a good relation with the potential of Mn/O-PCN. $^1\text{O}_2$ and electron transfer may contribute to the main degradation of ENR in Mn/O-PCN/PMS system. This study revealed the degradation mechanism of PMS activation by metal and oxygen co-doped carbon nitride catalyst for organic pollutant oxidation. In addition, there are still some drawbacks in this study, such as focusing on the single pollutant removal. In the future, appropriate catalysts should be designed according to the types of pollutants, and the active species produced by catalysts should be fully used.

Declaration of Competing Interest

The authors declare that they have no known competing financial interests or personal relationships that could have appeared to influence the work reported in this paper.

Acknowledgements

This study was financially supported by the Program for the National Natural Science Foundation of China (U20A20323, 52100182, 51879101, 51579098, 51779090, 51709101, 51521006, 51809090), China Postdoctoral Science Foundation (2021 T140192, 2021 M690054, 2021 M690961), the China National Postdoctoral Program for Innovative Talents (BX20200119), the Fundamental Research Funds for the Central Universities (531118010574) and the Science and Technology Innovation Program of Hunan Province (2020RC4014).

Appendix A. Supplementary data

Supplementary data to this article can be found online at <https://doi.org/10.1016/j.cej.2021.132751>.

References

- Y. Yang, X. Li, C. Zhou, W. Xiong, G. Zeng, D. Huang, C. Zhang, W. Wang, B. Song, X. Tang, X. Li, H. Guo, Recent advances in application of graphitic carbon nitride-based catalysts for degrading organic contaminants in water through advanced oxidation processes beyond photocatalysis: A critical review, *Water Res.* 184 (2020) 116200, <https://doi.org/10.1016/j.watres.2020.116200>.
- X. Ren, L. Tang, J. Wang, E. Almatrafi, H. Feng, X. Tang, J. Yu, Y. Yang, X. Li, C. Zhou, Z. Zeng, G. Zeng, Highly efficient catalytic hydrogenation of nitrophenols by sewage sludge derived biochar, *Water Res.* 201 (2021), 117360.
- B. Shao, H. Dong, L. Feng, J. Qiao, X. Guan, Influence of [sulfite]/[Fe(VI)] molar ratio on the active oxidants generation in Fe(VI)/sulfite process, *J. Hazard. Mater.* 384 (2020), 121303.
- E.D. Koutsouroubi, I. Vamvakakis, M.G. Minotaki, I.T. Papadas, C. Drivas, S. A. Choulis, G. Kopidakis, S. Kennou, G.S. Armatas, Ni-doped MoS₂ modified graphitic carbon nitride layered hetero-nanostructures as highly efficient photocatalysts for environmental remediation, *Appl. Catal. B-Environ.* 297 (2021), 120419.
- H. Wang, H. Wang, Z. Wang, L. Tang, G. Zeng, P. Xu, M. Chen, T. Xiong, C. Zhou, X. Li, D. Huang, Y. Zhu, Z. Wang, J. Tang, Covalent organic framework photocatalysts: structures and applications, *Chem. Soc. Rev.* 49 (12) (2020) 4135–4165.
- C. Huang, C. Zhang, D. Huang, D. Wang, S. Tian, R. Wang, Y. Yang, W. Wang, F. Qin, Influence of surface functionalities of pyrogenic carbonaceous materials on the generation of reactive species towards organic contaminants: A review, *Chem. Eng. J.* 404 (2021), 127066.
- S. Chen, D. Huang, G. Zeng, W. Xue, L. Lei, P. Xu, R. Deng, J. Li, M. Cheng, In-situ synthesis of facet-dependent BiVO₄/Ag₃PO₄/PANI photocatalyst with enhanced visible-light-induced photocatalytic degradation performance: Synergism of interfacial coupling and hole-transfer, *Chem. Eng. J.* 382 (2020), 122840.
- X. Li, X. Huang, S. Xi, S. Miao, J. Ding, W. Cai, S. Liu, X. Yang, H. Yang, J. Gao, J. Wang, Y. Huang, T. Zhang, B. Liu, Single cobalt atoms anchored on porous n-doped graphene with dual reaction sites for efficient fenton-like catalysis, *J. Am. Chem. Soc.* 140 (39) (2018) 12469–12475.
- C. Zhang, D. He, S. Fu, G. Zeng, Q. Liang, Y. Yang, D. Huang, W. Wang, Y. Zhou, Silver iodide decorated ZnSn(OH)₆ hollow cube: Room-temperature preparation and application for highly efficient photocatalytic oxytetracycline degradation, *Chem. Eng. J.* 421 (2021), 129810.
- S. Liu, Z. Zhang, F. Huang, Y. Liu, L. Feng, J. Jiang, L. Zhang, F. Qi, C. Liu, Carbonized polyaniline activated peroxymonosulfate (PMS) for phenol degradation: Role of PMS adsorption and singlet oxygen generation, *Appl. Catal. B-Environ.* 286 (2021), 119921.
- W. Ren, G. Nie, P. Zhou, H. Zhang, X. Duan, S. Wang, The intrinsic nature of persulfate activation and n-doping in carbocatalysis, *Environ Sci Technol* 54 (10) (2020) 6438–6447.
- S. Ye, M. Cheng, G. Zeng, X. Tan, H. Wu, J. Liang, M. Shen, B. Song, J. Liu, H. Yang, Y. Zhang, Insights into catalytic removal and separation of attached metals from natural-aged microplastics by magnetic biochar activating oxidation process, *Water Res.* 179 (2020), 115876.
- Y. Zhou, Y. Gao, S.-Y. Pang, J. Jiang, Y. Yang, J. Ma, Y. Yang, J. Duan, Q. Guo, Oxidation of fluoroquinolone antibiotics by peroxymonosulfate without activation: Kinetics, products, and antibacterial deactivation, *Water Res.* 145 (2018) 210–219.
- Y. Shang, X. Xu, B. Gao, S. Wang, X. Duan, Single-atom catalysis in advanced oxidation processes for environmental remediation, *Chem. Soc. Rev.* 50 (8) (2021) 5281–5322.
- R.M. Balakrishnan, I. Ilango, G. Gamana, X.-T. Bui, A. Pugazhendhi, Cobalt ferrite nanoparticles and peroxymonosulfate system for the removal of ampicillin from aqueous solution, *J. Water Pro. Eng.* 40 (2021), 101823.
- E. Saputra, S. Muhammad, H. Sun, H.M. Ang, M.O. Tadé, S. Wang, Different crystallographic one-dimensional MnO₂ nanomaterials and their superior performance in catalytic phenol degradation, *Environ. Sci. Technol.* 47 (11) (2013) 5882–5887.
- Z. Zhao, J. Zhao, C. Yang, Efficient removal of ciprofloxacin by peroxymonosulfate/Mn₃O₄-MnO₂ catalytic oxidation system, *Chem. Eng. J.* 327 (2017) 481–489.
- Y. Gao, Y. Zhou, S.-Y. Pang, J. Jiang, Y.-M. Shen, Y. Song, J.-B. Duan, Q. Guo, Enhanced peroxymonosulfate activation via complexed Mn(II): A novel non-radical oxidation mechanism involving manganese intermediates, *Water Res.* 193 (2021), 116856.
- C. Zhang, S. Tian, F. Qin, Y. Yu, D. Huang, A. Duan, C. Zhou, Y. Yang, W. Wang, Y. Zhou, H. Luo, Catalyst-free activation of permanganate under visible light irradiation for sulfamethazine degradation: Experiments and theoretical calculation, *Water Res.* 194 (2021), 116915.
- H. Zhou, J. Peng, J. Li, J. You, L. Lai, R. Liu, Z. Ao, G. Yao, B. Lai, Metal-free black-red phosphorus as an efficient heterogeneous reductant to boost Fe³⁺/Fe²⁺ cycle for peroxymonosulfate activation, *Water Res.* 188 (2021), 116529.
- T.T. Huo, G.M. Ba, Q.H. Deng, F. Yu, G.A. Wang, H.P. Li, W.G. Hou, A dual strategy for synthesizing carbon/defect comodified polymeric carbon nitride porous nanotubes with boosted photocatalytic hydrogen evolution and synchronous contaminant degradation, *Appl. Catal. B-Environ.* 287 (2021), 119995.
- J. Cao, W. Nie, L. Huang, Y. Ding, K. Lv, H. Tang, Photocatalytic activation of sulfite by nitrogen vacancy modified graphitic carbon nitride for efficient degradation of carbamazepine, *Appl. Catal. B-Environ.* 241 (2019) 18–27.
- C. Zhou, G. Zeng, D. Huang, Y. Luo, M. Cheng, Y. Liu, W. Xiong, Y. Yang, B. Song, W. Wang, B. Shao, Z. Li, Distorted polymeric carbon nitride via carriers transfer bridges with superior photocatalytic activity for organic pollutants oxidation and hydrogen production under visible light, *J. Hazard. Mater.* 386 (2020), 121947.
- A. Kumar, P. Raizada, P. Singh, R.V. Saini, A.K. Saini, A. Hosseini-Bandegharai, Perspective and status of polymeric graphitic carbon nitride based Z-scheme photocatalytic systems for sustainable photocatalytic water purification, *Chem. Eng. J.* 391 (2020), 123496.
- J. Miao, W. Geng, P.J.J. Alvarez, M. Long, 2D N-doped porous carbon derived from polydopamine-coated graphitic carbon nitride for efficient nonradical activation of peroxymonosulfate, *Environ Sci Technol* 54 (13) (2020) 8473–8481.
- Y. Gao, Y. Zhu, L. Lyu, Q. Zeng, X. Xing, C. Hu, Electronic structure modulation of graphitic carbon nitride by oxygen doping for enhanced catalytic degradation of organic pollutants through peroxymonosulfate activation, *Environ. Sci. Technol.* 52 (24) (2018) 14371–14380.
- J. Fan, H. Qin, S. Jiang, Mn-doped g-C₃N₄ composite to activate peroxymonosulfate for acetaminophen degradation: The role of superoxide anion and singlet oxygen, *Chem. Eng. J.* 359 (2019) 723–732.
- S. Wang, Y. Liu, J. Wang, Peroxymonosulfate activation by Fe-co-o-codoped graphitic carbon nitride for degradation of sulfamethoxazole, *Environ Sci Technol* 54 (16) (2020) 10361–10369.
- Y. Oh, J.O. Hwang, E.-S. Lee, M. Yoon, V.-D. Le, Y.-H. Kim, D.H. Kim, S.O. Kim, Divalent Fe atom coordination in two-dimensional microporous graphitic carbon nitride, *ACS Appl. Mater. Interfaces.* 8 (38) (2016) 25438–25443.
- H. Li, C. Shan, B. Pan, Fe(III)-Doped g-C₃N₄ mediated peroxymonosulfate activation for selective degradation of phenolic compounds via high-valent iron-oxo species, *Environ. Sci. Technol.* 52 (4) (2018) 2197–2205.
- F. Chen, L.L. Liu, J.J. Chen, W.W. Li, Y.P. Chen, Y.J. Zhang, J.H. Wu, S.C. Mei, Q. Yang, H.Q. Yu, Efficient decontamination of organic pollutants under high salinity conditions by a nonradical peroxymonosulfate activation system, *Water Res.* 191 (2021), 116799.
- H. Guo, C.-G. Niu, C. Liang, H.-Y. Niu, Y.-Y. Yang, H.-Y. Liu, N. Tang, H.-X. Fang, Highly crystalline porous carbon nitride with electron accumulation capacity: Promoting exciton dissociation and charge carrier generation for photocatalytic molecular oxygen activation, *Chem. Eng. J.* 409 (2021), 128030.
- G. Peng, T. Li, B. Ai, S. Yang, J. Fu, Q. He, G. Yu, S. Deng, Highly efficient removal of enrofloxacin by magnetic montmorillonite via adsorption and persulfate oxidation, *Chem. Eng. J.* 360 (2019) 1119–1127.
- X. Zhou, Z. Zeng, G. Zeng, C. Lai, R. Xiao, S. Liu, D. Huang, L. Qin, X. Liu, B. Li, H. Yi, Y. Fu, L. Li, M. Zhang, Z. Wang, Insight into the mechanism of persulfate activated by bone char: Unraveling the role of functional structure of biochar, *Chem. Eng. J.* 401 (2020), 126127.
- W. Xing, W. Tu, Z. Han, Y. Hu, Q. Meng, G. Chen, Template-induced high-crystalline g-c3n4 nanosheets for enhanced photocatalytic h2 evolution, *ACS Energy Letters* 3 (3) (2018) 514–519.
- Y. Liu, J. Luo, L. Tang, C. Feng, J. Wang, Y. Deng, H. Liu, J. Yu, H. Feng, J. Wang, Origin of the enhanced reusability and electron transfer of the carbon-coated Mn₃O₄ nanocube for persulfate activation, *ACS Catalysis* 10 (24) (2020) 14857–14870.
- Z.-Y. Guo, C.-X. Li, M. Gao, X. Han, Y.-J. Zhang, W.-J. Zhang, W.-W. Li, Mn@O covalency governs the intrinsic activity of co-mn spinel oxides for boosted peroxymonosulfate activation, *Angew. Chem. Int. Ed.* 60 (1) (2021) 274–280.
- X. Song, X. Li, X. Zhang, Y. Wu, C. Ma, P. Huo, Y. Yan, Fabricating C and O codoped carbon nitride with intramolecular donor-acceptor systems for efficient photoreduction of CO₂ to CO, *Appl. Catal. B-Environ.* 268 (2020), 118736.
- X. Du, X. Bai, L. Xu, L. Yang, P. Jin, Visible-light activation of persulfate by TiO₂/g-C₃N₄ photocatalyst toward efficient degradation of micropollutants, *Chem. Eng. J.* 384 (2020), 123245.
- J. Jiang, X. Wang, C. Zhang, T. Li, Y. Lin, T. Xie, S. Dong, Porous 0D/3D NiCo₂O₄/g-C₃N₄ accelerate emerging pollutant degradation in PMS/vis system: Degradation mechanism, pathway and toxicity assessment, *Chem. Eng. J.* 397 (2020), 125356.
- F. Wang, Y. Feng, P. Chen, Y. Wang, Y. Su, Q. Zhang, Y. Zeng, Z. Xie, H. Liu, Y. Liu, W. Lv, G. Liu, Photocatalytic degradation of fluoroquinolone antibiotics using ordered mesoporous g-C₃N₄ under simulated sunlight irradiation: Kinetics, mechanism, and antibacterial activity elimination, *Appl. Catal. B-Environ.* 227 (2018) 114–122.
- S. Yanan, X. Xing, Q. Yue, B. Gao, Y. Li, Nitrogen-doped carbon nanotubes encapsulating Fe/Zn nanoparticles as a persulfate activator for sulfamethoxazole degradation: role of encapsulated bimetallic nanoparticles and nonradical reaction, *Environ. Sci.: Nano* 7 (2020) 1444–1453.
- J. Luo, S. Bo, Q. An, Z. Xiao, H. Wang, W. Cai, S. Zhai, Z. Li, Designing ordered composites with confined Co-N/C layers for efficient pollutant degradation: Structure-dependent performance and PMS activation mechanism, *Micropor. Mesopor. Mater.* 293 (2020) 109810, <https://doi.org/10.1016/j.micromeso.2019.109810>.
- X.-H. Yi, H. Ji, C.-C. Wang, Y. Li, Y.-H. Li, C. Zhao, A.o. Wang, H. Fu, P. Wang, X. u. Zhao, W. Liu, Photocatalysis-activated SR-AOP over PDINH/MIL-88A(Fe) composites for boosted chloroquine phosphate degradation: Performance, mechanism, pathway and DFT calculations, *Appl. Catal. B-Environ.* 293 (2021) 120229, <https://doi.org/10.1016/j.apcatb.2021.120229>.

- [45] M. Li, H. Zhong, Z. He, L. Hu, W. Sun, P. Loganathan, D. Xiong, Degradation of various thiol collectors in simulated and real mineral processing wastewater of sulfide ore in heterogeneous modified manganese slag/PMS system, *Chem. Eng. J.* 413 (2021), 127478.
- [46] Y. Yang, P. Zhang, K. Hu, X. Duan, Y. Ren, H. Sun, S. Wang, Sustainable redox processes induced by peroxymonosulfate and metal doping on amorphous manganese dioxide for nonradical degradation of water contaminants, *Appl. Catal. B-Environ.* 286 (2021), 119903.
- [47] L. Wang, H. Xu, N. Jiang, Z. Wang, J. Jiang, T. Zhang, Trace cupric species triggered decomposition of peroxymonosulfate and degradation of organic pollutants: cu(III) being the primary and selective intermediate oxidant, *Environ. Sci. Technol.* 54 (2020) 4686–4694.
- [48] G. Fang, J. Gao, D.D. Dionysiou, C. Liu, D. Zhou, Activation of persulfate by quinones: free radical reactions and implication for the degradation of pcbs, *Environ. Sci. Technol.* 47 (2013) 4605–4611.
- [49] N. Jiang, H. Xu, L. Wang, J. Jiang, T. Zhang, Nonradical oxidation of pollutants with single-atom-Fe(III)-activated persulfate: Fe(V) being the possible intermediate oxidant, *Environ. Sci. Technol.* 54 (2020) 14057–14065.
- [50] H.-B. Qiu, P.-C. Guo, L.i. Yuan, G.-P. Sheng, Different non-radical oxidation processes of persulfate and peroxymonosulfate activation by nitrogen-doped mesoporous carbon, *Chin. Chem. Lett.* 31 (10) (2020) 2614–2618.
- [51] P. Duan, Y. Qi, S. Feng, X. Peng, W. Wang, Y. Yue, Y. Shang, Y. Li, B. Gao, X. Xu, Enhanced degradation of clothianidin in peroxymonosulfate/catalyst system via core-shell FeMn @ N-C and phosphate surrounding, *Appl. Catal. B-Environ.* 267 (2020), 118717.
- [52] L. Peng, Y. Shang, B. Gao, X. Xu, Co₃O₄ anchored in N, S heteroatom co-doped porous carbons for degradation of organic contaminant: role of pyridinic N-Co binding and high tolerance of chloride, *Appl. Catal. B-Environ.* 282 (2021), 119484.
- [53] L. Peng, X. Duan, Y. Shang, B. Gao, X. Xu, Engineered carbon supported single iron atom sites and iron clusters from Fe-rich Enteromorpha for Fenton-like reactions via nonradical pathways, *Appl. Catal. B-Environ.* 287 (2021), 119963.
- [54] B. Yang, R.S. Kookana, M. Williams, G.G. Ying, J. Du, H. Doan, A. Kumar, Oxidation of ciprofloxacin and enrofloxacin by ferrate(VI): Products identification, and toxicity evaluation, *J Hazard Mater* 320 (2016) 296–303.
- [55] R. Du, P. Chen, Q. Zhang, G. Yu, The degradation of enrofloxacin by a non-metallic heptazine-based OCN polymer: Kinetics, mechanism and effect of water constituents, *Chemosphere* 273 (2021), 128435.
- [56] A. Wang, H. Wang, H. Deng, S. Wang, W. Shi, Z. Yi, R. Qiu, K. Yan, Controllable synthesis of mesoporous manganese oxide microsphere efficient for photo-Fenton-like removal of fluoroquinolone antibiotics, *Appl. Catal. B-Environ.* 248 (2019) 298–308.
- [57] P. Qiu, C. Xu, H. Chen, F. Jiang, X. Wang, R. Lu, X. Zhang, One step synthesis of oxygen doped porous graphitic carbon nitride with remarkable improvement of photo-oxidation activity: Role of oxygen on visible light photocatalytic activity, *Appl. Catal. B-Environ.* 206 (2017) 319–327.